

Multipole decomposition of the $^{16}\text{O}(p, n)^{16}\text{F}$ and $^{18}\text{O}(p, n)^{18}\text{F}$ reactions at 494 MeV

D. J. Mercer,¹ J. Rapaport,² C. A. Whitten, Jr.,³
 D. Adams,⁴ R. Byrd,⁵ X. Y. Chen,¹ A. Fazely,⁶ T. Gaussiran,⁴ E. Gülmez,^{3,*}
 C. Goodman,⁷ D. W. Huang,⁷ G. Igo,³ A. Ling,^{5,†} D. Marchlinski,⁸
 D. Prout,^{1,8} L. Rybarczyk,⁵ E. Sugarbaker,⁸ and T. N. Taddeucci⁵

¹University of Colorado, Boulder, Colorado 80309

²Ohio University, Athens, Ohio 45701

³University of California, Los Angeles, California 90024

⁴Rice University, Houston, Texas 77251

⁵Los Alamos National Laboratory, Los Alamos, New Mexico 87545

⁶Louisiana State University, Baton Rouge, Louisiana 70803

⁷Indiana University Cyclotron Facility, Bloomington, Indiana 47405

⁸The Ohio State University, Columbus, Ohio 43210

(Received 22 February 1994)

Measurements of the differential cross section for the $^{16}\text{O}(p, n)^{16}\text{F}$ and $^{18}\text{O}(p, n)^{18}\text{F}$ reactions are made at $\theta_{\text{lab}} = 0^\circ, 1^\circ, 2^\circ, 3^\circ, 4^\circ, 6^\circ,$ and 8° with a bombardment energy of 494 MeV. Multipole decomposition methods based on the measured angular distributions are used to extract $\Delta L = 0,$ $\Delta L = 1,$ and $\Delta L = 2$ contributions to the cross sections. The summed Gamow-Teller strength $B(\text{GT})$ is computed for the excitation energy region 0–30 MeV in ^{16}F , and 0–12.5 MeV in ^{18}F . Difficulties with the decomposition methods are discussed.

PACS number(s): 25.40.Kv, 27.20.+n

I. INTRODUCTION

Models and our views on the structure of nuclei are primarily tested in light nuclei. In particular, ^{16}O , which in the simplest shell model is a spin saturated doubly magic nucleus, has received a large share of theoretical interest. At an earlier stage, Brown and Green [1] gave a successful and important description of the low-lying excited states using a $(0 + 2 + 4)\hbar\omega$ model space. More recently, studies on ^{16}O done by Haxton and Johnson [2] and Warburton and Brown [3] have reaffirmed the above description of the low-lying levels.

Charge-exchange reactions are excellent probes to study correlations in the ground state wave function of a given nucleus. In particular, the excitation via the $^{16}\text{O}(p, n)^{16}\text{F}$ reaction of transitions characterized as Gamow-Teller (GT) with $\Delta J^\pi = 1^+, \Delta L = 0, \Delta S = 1$ provides a unique way to study $(2 + 4)\hbar\omega$ admixtures in the ground state wave function of ^{16}O , since in the simple $0\hbar\omega$ model space, no GT transitions are allowed.

In recent years, many advances have been made in the study of GT transitions by using the (p, n) reaction at intermediate energies. In the energy range 160–500 MeV, the (p, n) reaction has been used to excite the nuclear spin response, using the dominance of the spin-isospin

term $(\sigma \cdot \tau)$ in the effective nucleon-nucleon interaction. The present measurements attempt to determine the GT strength for ^{16}F from angular distributions obtained in the $^{16}\text{O}(p, n)^{16}\text{F}$ reaction at 494 MeV. Explicit calculations of the strength have been done by Arima and Strottman [4], by Snover *et al.* [5], and more recently by Haxton and Johnson [2]. The last calculation predicts a summed GT strength of about 0.7 unit (units for which the free neutron decay has a GT strength equal to 3) for ^{16}F excitation energies up to 40 MeV.

Earlier measurements for GT strength in the $A = 16$ system were done by inelastic scattering and charge-exchange reactions. In a $^{16}\text{O}(p, p')$ study at $E_p = 201$ MeV reported by Djalali *et al.* [6], three transitions are identified to $T = 1, J = 1^+$ final states in ^{16}O in the excitation energy region between 16 and 19 MeV. The same states have been previously reported by Küchler *et al.* [7] in back-angle inelastic electron scattering and by Snover *et al.* [5] in their $^{15}\text{N}(p, \gamma)$ work. Analogs to these states in the ^{16}F nucleus are also reported by Fazely *et al.* [8] in the study of the $^{16}\text{O}(p, n)^{16}\text{F}$ reaction at $E_p = 135$ MeV.

More recent measurements of the $^{16}\text{O}(n, p)^{16}\text{N}$ reaction at $E_n = 298$ MeV have been reported by Hicks *et al.* [9] where, using a multipole decomposition technique, transitions characterized with an angular momentum transfer $L = 0$ are identified to obtain the GT strength distribution. Because of a 1.2 MeV energy resolution, regions of concentration of $L = 0$ transitions are identified, rather than individual states.

For experimental reasons, the spectroscopy of ^{16}N is better known than that of ^{16}F [10]. Much of the spectroscopic information about excited states in ^{16}F has been obtained from a high resolution time-of-flight measure-

*Present address: Physics Department, Bogazici University, PK 2, Bebek 80815, Istanbul, Turkey.

†Present address: TRIUMF Laboratory, Vancouver, B.C., Canada V6T 2A3.

ment of the $^{14}\text{N}(^3\text{He},n)^{16}\text{F}$ reaction reported by Bohne *et al.* [11]. In particular, two excited states at 3.751 MeV and 4.646 MeV excitation energy are found to be $J^\pi = 1^+$. In addition, a state at 6.23 MeV is also identified as a 1^+ state in the $^{16}\text{O}(p,n)^{16}\text{F}$ work by Fazely *et al.* [8]. Snover *et al.* [5] and Rapaport [12] have estimated the corresponding GT strengths. Values for the GT strength of ~ 0.006 , 0.09, and 0.075, in the units indicated above, are estimated for the corresponding transitions. A discrepancy [5] between $2\hbar\omega$ shell-model calculations and the above experimental $B(\text{GT})$ strength below 7 MeV in ^{16}F has not yet been fully removed even in the more complete calculations of Haxton and Johnson [2]. These calculations are necessary to estimate the total GT strength that may reside up to 50 MeV of excitation in ^{16}F .

The GT strength function for the $^{16}\text{O}(p,n)^{16}\text{F}$ reaction up to excitation energies of about 50 MeV has interest beyond specific nuclear structure questions. A precision measurement of the Weinberg angle has been proposed [13] which extracts this quantity from measurements of neutrino-electron elastic scattering in a water Čerenkov detector. In these measurements, the reaction $\nu_e + ^{16}\text{O} \rightarrow ^{16}\text{F} + e^-$ proceeding by the GT operator is an important background, since the electron from this reaction emits Čerenkov light just as a recoil electron from ν_e - e elastic scattering.

In the present study we report measurements of the differential cross section for the $^{16,18}\text{O}(p,n)^{16,18}\text{F}$ reactions at angles θ_{lab} between 0° and 8° . The measurements were done at $E_p = 494$ MeV using the LAMPF/NTOF facilities. A multipole decomposition technique is used to analyze the angular distributions and to obtain transitions characterized with an angular momentum transfer $L = 0$. The $L = 0$ differential cross section for the $^{18}\text{O}(p,n)^{18}\text{F}(\text{g.s.})$ transition with an empirically known $B(\text{GT})$ value is used to normalize the deduced $L = 0$ cross section in the $^{16}\text{O}(p,n)^{16}\text{F}$ reaction in $B(\text{GT})$ units. The energy dependence of the resulting GT strength is compared with theoretical calculations of Haxton and Johnson [2].

An intrinsic advantage of the $^{16}\text{O}(p,n)^{16}\text{F}$ reaction at $E_p = 495$ MeV is the fact that at zero degrees the momentum transfer q for the ground state transition is 0.10 fm^{-1} while at $E_p = 135$ MeV it is 0.17 fm^{-1} . At the higher energy this provides a better sensitivity to differentiate between $L = 0$ and $L = 1$ momentum transfers, and thus to identify better weak GT transitions in regions of strong dipole and spin-dipole excitation.

II. EXPERIMENTAL METHODS AND DATA ANALYSIS

A. Apparatus

1. Proton beam and swinger cave

The Neutron Time-of-Flight (NTOF) facility at the Los Alamos Meson Physics Facility (LAMPF) was used for the measurements. A proton beam with mean kinetic energy 494.0 ± 0.5 MeV and an average current of about 30 nA was produced in the LAMPF LINAC. The beam was pulsed in 400 μs bursts at a frequency of 10 Hz, and each burst had an internal ‘‘micropulse’’ period of 2146.6 ns. To produce a nearly isochronous beam, postacceleration longitudinal focusing (rebunching) was performed using accelerator modules not needed for acceleration [14]. In the swinger cave the proton beam was steered by a series of magnets to strike the target at the desired angle, as depicted schematically in Fig. 1. Neutrons from (p,n) reactions scattered at an angle θ_{lab} traveled along a 341.6-m outdoor flight path before reaching the detector. Beam steering was necessary because the neutron collimator, flight path, and detector lie in a fixed direction. Protons downstream from the target were swept by a movable dipole magnet into an electrically isolated graphite beam stop connected to a current integrator. A secondary emission monitor (SEM) located upstream from the target was also helpful for monitoring the beam current.

2. Target

The primary target was a disk of ice which filled a 3.81 cm diameter hole in a 0.318 cm thick copper plate mounted perpendicular to the beam. This plate was maintained at a temperature of -65°C with a commercially available cooling system (FTS Flexi-Cool System FC-20-84-P2S). Aluminized Mylar windows of 7.6 μm thickness were used to prevent sublimation losses. The ice target design is described in greater detail in [15]. Previous $^{16}\text{O}(p,n)^{16}\text{F}$ measurements [8] used BeO targets and had to deal with a large background from $^9\text{Be}(p,n)^9\text{B}$ reactions. The H_2O target used in the present experiment significantly reduced the background. Hydrogen itself can produce neutrons only via the $p+p \rightarrow n + p + \pi^+$ reaction with a Q value of -140.8 MeV.

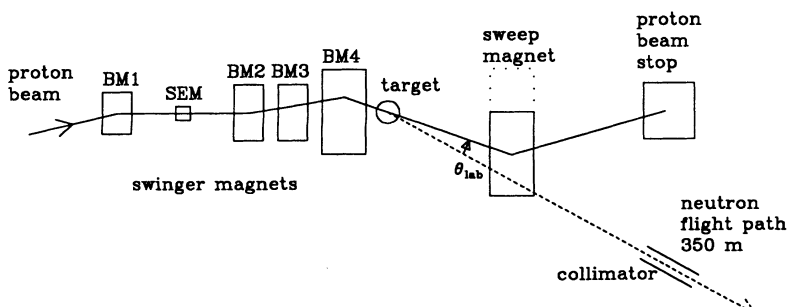


FIG. 1. Schematic of the NTOF swinger cave at LAMPF.

A small amount of ^{18}O -enriched water was added to the natural water used in the target, yielding a $^{16}\text{O}:^{17}\text{O}:^{18}\text{O}$ ratio of 0.947:0.001:0.052 and an effective thickness for ^{16}O of 246 mg/cm^2 . The $^{18}\text{O}(p,n)^{18}\text{F}$ reaction has a very strong GT transition to the 1^+ ^{18}F ground state, and the peak corresponding to this transition ($Q = -2.44\text{ MeV}$) is well separated from any neutron yield from the $^{16}\text{O}(p,n)$ reaction ($Q = -16.21\text{ MeV}$). The $^{18}\text{O}(p,n)^{18}\text{F}$ ground state peak in the $^{16}\text{O}(p,n)$ neutron spectrum served several purposes. One, it provided a quick online check for the operation of the complete data acquisition system. Two, it provided a normalization peak to check for possible sublimation of the ice target during the data taking period ($\sim 1\text{ week}$), and three, its angular distribution provided a nearly pure $L = 0$ GT transition for relative angular normalization.

An ice target made from undiluted ^{18}O -enriched water was also used. For this target the isotopic ratio was $^{16}\text{O}:^{17}\text{O}:^{18}\text{O} = 0.032:0.012:0.956$ and the effective ^{18}O thickness was 278 mg/cm^2 .

Background contributions to the (p,n) spectra from the ^{16}O target were obtained from the ^{18}O target, from a Mylar target with 50 layers of $7.6\text{ }\mu\text{m}$ thick foil, from a target of 27.5 mil copper, and from a “hole” target which was a replica of the copper plates used for the ^{16}O and ^{18}O targets but without ice or windows. Measurements of (p,n) yields from the “hole” target were used at each θ_{lab} setting to minimize and monitor the beam halo striking the copper plate. The ^{18}O target was also used to obtain high statistics data for $^{18}\text{O}(p,n)$ angular distributions. All these targets were mounted on a ladder along with a ^7Li target of thickness 721 mg/cm^2 used to obtain absolute (p,n) cross sections, as discussed below. For a given θ_{lab} setting data runs on the ^{16}O and ^{18}O targets were interspersed with runs from the various targets providing information on the background contributions.

3. Detector

Neutrons were detected in the NTOF polarimeter, operated in the singles (nonpolarimetry) mode. As presented in Fig. 2, the detector consisted of three tanks of BC-517S mineral-oil-based scintillator, each tank measuring $10\text{ cm} \times 100\text{ cm} \times 107\text{ cm}$, oriented perpendicular to the beam. Each tank was subdivided into ten optically isolated cells measuring $10\text{ cm} \times 10\text{ cm} \times 107\text{ cm}$, and each cell was viewed by phototubes at both ends. Flight times were determined by comparing timing signals from the phototubes with an accelerator-generated rf synchronization signal, and the overall timing calibration was performed using gamma rays from $^{16}\text{O}(p,\gamma x)$ events, which travel from the target with velocity c . The time-of-flight window for high energy neutrons was about 110 ns wide, corresponding to neutron energies between about 415 MeV and 550 MeV . This permitted the study of $^{16}\text{O}(p,n)^{16}\text{F}$ transitions up to excitation energies of at least 60 MeV . Neutron kinetic energies were calculated from the flight times with a FWHM resolution of 1.1 MeV . Thin (0.3 cm) planes of plastic scintillator were used to tag and reject charged particles produced by

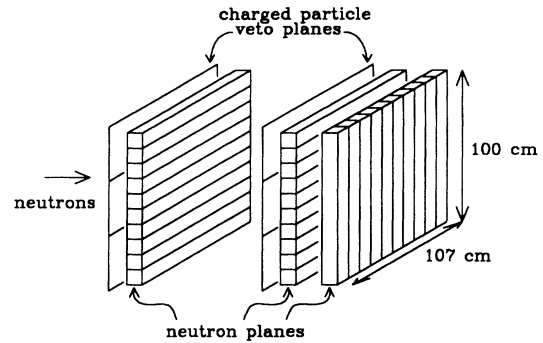


FIG. 2. NTOF neutron detector. Phototubes have been omitted for clarity.

charge-exchange scattering along the flight path. The NTOF detector is described in greater detail elsewhere [16,17]. Data acquisition employed a “Q”-based system, described in detail in Ref. [18].

B. Data reduction

1. Normalization

The expected relationship between the observed number of neutrons N_{obs} and the differential cross section is given by

$$d\sigma_{\text{lab}}(\theta)/d\Omega = N_{\text{obs}}/[I(\rho x N_0/A)\Delta\Omega\epsilon T f_l], \quad (2.1)$$

where I is the number of incident protons, $\rho x N_0/A$ is the target thickness in nuclei/ cm^2 , $\Delta\Omega$ is the solid angle subtended by the detector ($8.6\text{ }\mu\text{sr}$), ϵ is the intrinsic detector efficiency for neutron singles ($\approx 20\%$), T is the transmission factor along the flight path ($\approx 63\%$ for $450\text{--}500\text{ MeV}$ neutrons), and f_l is the detector live fraction ($\approx 75\%$).

The target-independent constants $\Delta\Omega$, ϵ , and T are difficult to measure independently, so we determine the value of the product of these three constants by measuring the yield from a ^7Li target and using the known zero-degree $^7\text{Li}(p,n)^7\text{Be}$ (g.s. $+0.43\text{ MeV}$) cross section, $\sigma_{\text{c.m.}}(0^\circ) = 27.0 \pm 1.0\text{ mb/sr}$ at 494 MeV [19].

The integrated beam current I was monitored using the graphite beam stop attached to a current integrator. This “Faraday cup” system was found to be nonlinear at the 20% level with respect to beam intensity. Although the SEM gave a better measure of beam intensity, it introduced a beam halo that could be detected using the “hole” target. It was sufficient to renormalize the “Faraday cup” readings to a beam intensity standard determined with the SEM.

At high data rates, when the probability of receiving more than one neutron from a given micropulse is not negligible, the system becomes biased toward faster (higher energy) neutrons, since the data acquisition system will become busy on the first neutron and will not respond to the later (slower) neutron. An additional source of spectral distortion is a resolving time effect. If two

nonadjacent cells in a given plane are triggered within ~ 50 ns, this is seen as a single, invalid event, and rejected. This might occur if the spectrum contains a very strong, sharp peak. Thus, at high data rates, the relative counting loss in any sharp peak can be greater than the counting loss in the rest of the spectrum.

Algorithms based on methods described in the literature [20,21] were derived to correct for these spectral distortions. The study of these distortions was aided by the fact that (p,n) data with the ^7Li and ^{18}O targets had been taken at both low and high data acquisition rates (high and low live fractions, respectively) so that our algorithms could be tested empirically. The $^{16}\text{O}(p,n)$ data were taken at moderate data acquisition rates; therefore the corrections for spectral distortions were not large ($\leq 4\%$).

The energy scale for the data was aligned from run to run within a given setting of θ_{lab} (there were typically ten data runs with the ^{16}O target at each angle). For almost all the data the energy shifts were found to be minimal (≤ 100 keV). The energy scale was also aligned from angle to angle. Apart from recoil energy corrections, the angle-to-angle shifts were smaller than 200 keV, except for a 900 keV shift at 3° .

2. Background contributions

The most significant background contributions to the (p,n) spectra from the ^{16}O ice target were $^{18}\text{O}(p,n)^{18}\text{F}$ transitions from the isotopic mixture in this target, $^{12}\text{C}(p,n)^{12}\text{N}$ transitions from the Mylar foil target windows and from oil condensed on these foils, and $^{\text{nat}}\text{Cu}(p,n)\text{Zn}$ transitions from beam halo scattering on the plate surrounding the disk of ice. These background spectra, suitably normalized and with energy-loss corrections, were subtracted from the ^{16}O ice target (p,n) spectra. Similar procedures were carried out for the ^{18}O ice target (p,n) spectra.

The presence of oil condensed on the Mylar foil windows was inferred from the fact that a residual background was found in a region corresponding to ^{16}F excitation energies between 1 and 3 MeV. There are no known ^{16}F states in this region [10]. This is just the region where the strong $^{12}\text{C}(p,n)^{12}\text{N}$ 1^+ ground state transition is located (with $Q = -18.13$ MeV). The ^{12}C background contribution from the oil was obtained from a fitting routine using Mylar (p,n) spectra and demanding that the $\theta_{\text{lab}} = 0^\circ$ (p,n) spectra from the ^{16}O ice target be negligible at an excitation in ^{16}F of ~ 2 MeV. During the running period for this experiment two sets of $^{16}\text{O}(p,n)$ data were obtained at $\theta_{\text{lab}} = 0^\circ$, taken at the beginning and near the end of the running period, respectively. Comparison of these two data sets gave no evidence for contaminant increase during the running period.

A raw neutron energy spectrum from the ^{16}O ice target is presented in Fig. 3, along with the contributions from these three sources of background shown to scale. “Wrap-around” neutrons, which are slow neutrons produced in previous beam micropulses, were effectively eliminated using a software threshold for phototube pulse heights; the “wrap arounds” had a maximum kinetic energy of only 55 MeV.

3. Cross sections

The center-of-momentum differential cross sections as a function of angle and excitation energy are shown for the $^{16}\text{O}(p,n)^{16}\text{F}$ and for the $^{18}\text{O}(p,n)^{18}\text{F}$ reactions in Fig. 4 and in Fig. 5 respectively for $\theta_{\text{c.m.}} = 0^\circ, 1.1^\circ, 2.2^\circ, 3.3^\circ, 4.4^\circ, 6.6^\circ,$ and 8.8° . In addition to the statistical error (typically 2% for a 0.2 MeV bin), there is a 1.5% uncertainty in the determination of integrated current I for each angle. Normalization uncertainties include the ^7Li calibration (3%) and target thickness (3%), but since these are common to all angles there is little effect on the multipole decomposition (MD) analyses.

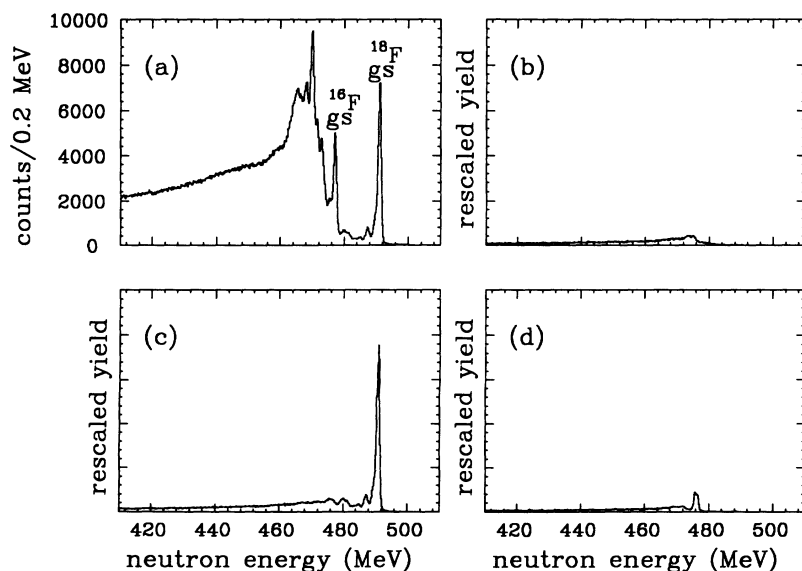


FIG. 3. (a) Raw neutron spectrum from the ^{16}O ice target at $\theta_{\text{lab}} = 1^\circ$; (b) “empty frame” background due primarily to beam halo striking the $^{\text{nat}}\text{Cu}$ target frame; (c) ^{18}O background due to the isotopic mixture of the target; (d) “window” background due to ^{12}C in the Mylar target windows and oil which had condensed on the windows. All backgrounds are shown with a scale appropriate to (a).

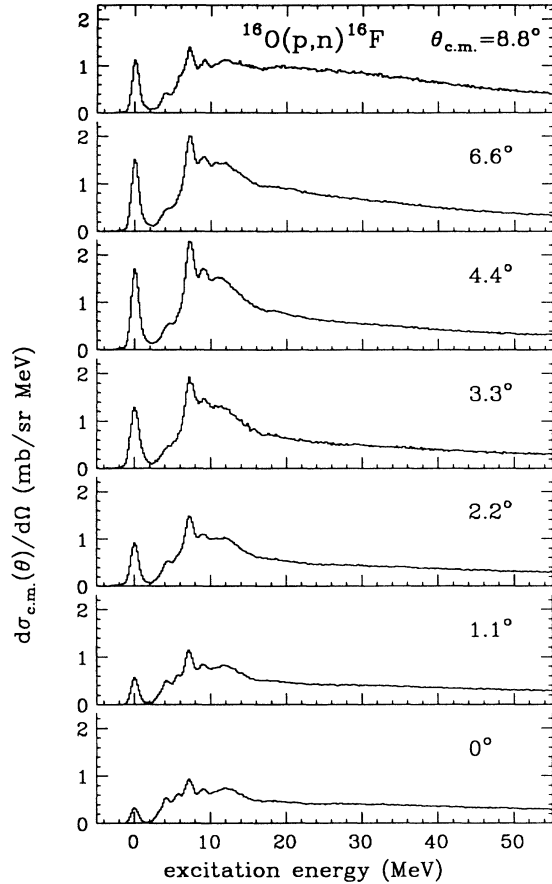


FIG. 4. Differential cross sections from the $^{16}\text{O}(p,n)^{16}\text{F}$ reaction at $E_p = 494$ MeV.

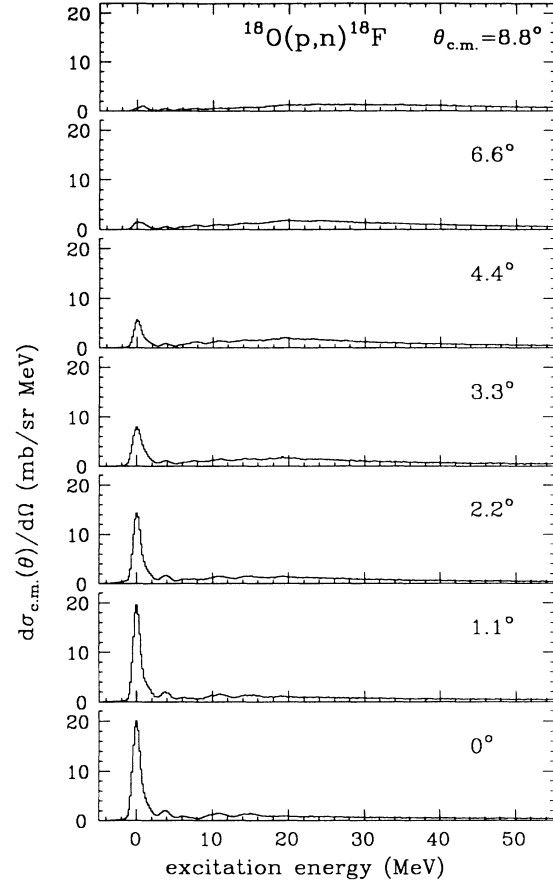


FIG. 5. Differential cross sections from the $^{18}\text{O}(p,n)^{18}\text{F}$ reaction at $E_p = 494$ MeV.

III. RESULTS

In this section we present theoretical analyses including the results of a multipole decomposition analysis.

A. Theoretical calculations

The differential cross sections were calculated using a distorted-wave impulse approximation (DWIA) with the code DW81 [22], which includes exchange. The inputs to such calculations are (a) an effective nucleon-nucleon interaction for which we have chosen the Franey and Love [23] parametrization of the free-nucleon interaction, (b) optical potential parameters, and (c) one-body density-matrix elements (OBDM's) from a nuclear structure calculation and single-particle wave functions for the nucleons involved in the transition.

Optical potential parameters are needed to calculate the distortions in the incident and outgoing channels. These were obtained from a microscopic optical potential by Flanders *et al.* [24] which is derived using an empirical effective interaction. This optical potential fits well the measured 500 MeV proton elastic scattering from ^{16}O . Other potentials that fit equally well the elastic scattering [25] produce similar (p, n) differential cross sections.

It is interesting to note that plane-wave impulse approximation (PWIA) and DWIA calculations produce differential cross sections with similar shapes in the angular range of the measured angular distribution, indicating low sensitivity at this energy to different sets of optical potentials.

The OBDM's for the $^{16}\text{O}(p, n)^{16}\text{F}$ reactions were obtained from the shell-model code OXBASH [26] in the p -shell and sd -shell (PSD) model space with the Millener-Kurath interaction [27]. The $L = 1$ calculations allowed up to two particles from each of the $p_{3/2}$ and $p_{1/2}$ orbitals to occupy the sd shell orbitals. The positive parity OBDM's for the $^{18}\text{O}(p, n)^{18}\text{F}$ reaction were also obtained from the shell-model code OXBASH. In this case we used a $0\hbar\omega$ calculation within the complete sd -shell model space and the Brown and Wildenthal interaction [28]. The single-particle radial wave functions were assumed to have a harmonic-oscillator (HO) shape with the size parameter $\alpha = 0.588 \text{ fm}^{-1}$. Calculations were also done in which these single-particle wave functions were generated from a Woods-Saxon (WS) potential, the depth of which was adjusted to reproduce the binding energies. For the $p_{1/2}$ and $p_{3/2}$ neutron hole wave functions, these energies were taken as the experimental separation energies 15.669 MeV ($p_{1/2}$) and 21.845 MeV ($p_{3/2}$), respectively. The proton particle is always unbound and its binding energy

was set at -0.010 MeV. No major changes in the shape of the $L = 1$ calculated differential cross sections were observed in the calculations done with HO or WS single-particle wave functions. However, the magnitudes for the cross sections calculated using the WS single-particle orbitals were larger by about 30% than those calculated with the HO shape.

B. The $^{16}\text{O}(p,n)^{16}\text{F}$ reaction

1. Excitation of the quartet of low-lying states in ^{16}F

Several authors have studied the nuclear structure of the low-lying states in ^{16}F [10]. The ground state ($J^\pi = 0_1^-$) and the 0.192 MeV state ($J^\pi = 1_1^-$) are calculated to have an almost pure ($1p_{1/2}^{-1}, 2s_{1/2}$) configuration, while the 0.424 MeV state ($J^\pi = 2_1^-$) and the 0.722 MeV state ($J^\pi = 3_1^-$) are calculated to have an almost pure ($1p_{1/2}^{-1}, 1d_{5/2}$) configuration [3]. These wave functions may be then considered well known and provide an excellent set of states to test the DWIA calculations. Also, from the empirical point of view, this quartet of states is well separated from the next excited state in ^{16}F at 3.76 MeV [10], allowing us in the present experiment to obtain its yield without interference from higher excited states. The present resolution is not sufficient to separate individual transitions, but as seen in Fig. 6 the main contribution (about 75% of the total calculated differential cross section) corresponds to that of the 2_1^- state. The calculated 0_1^- and 1_1^- transitions contribute in about equal amounts (approximately 12% each) to the total differential cross section up to $\theta_L = 4^\circ$. Orihara *et al.* [29] have measured individual angular distributions to the four members of the quartet excited in the $^{16}\text{O}(p,n)^{16}\text{F}$ reaction at $E_p = 35$ MeV with 60 keV neutron energy resolution. The reported relative yields for

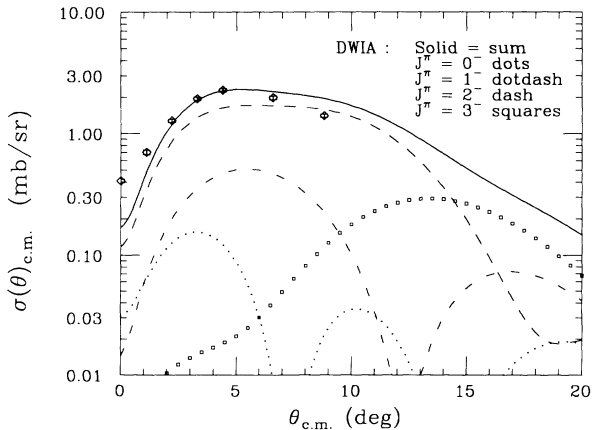


FIG. 6. Measured angular distribution for the neutron group near the ground state in ^{16}F excited via the $^{16}\text{O}(p,n)$ reaction at 494 MeV (diamonds with 1σ error bars). The curves are DWIA calculations corresponding to transitions to the 0_1^- , 1_1^- , 2_1^- , and 3_1^- states, each multiplied by a factor of 0.7. The solid curve represents the sum of the four different J^π contributions.

the 0^- , 1^- , and 2^- transitions are in general agreement with the results of the above calculations.

The DWIA calculations in Fig. 6 have been obtained with the optical model potential (OMP) of Flanders *et al.* [24] and one-particle-one-hole OBDME's provided by Millener [30]. These calculations, normalized by a factor of 0.7, agree with data at the peak of the angular distribution but disagree by almost a factor of 2 at $\theta = 0^\circ$. The calculations indicate that the shape of the observed ($0^\circ < \theta < 10^\circ$) angular distribution for this set of states is mainly due to the spin-dipole transition to the 2^- state at 0.424 MeV. This is expected because at these intermediate energies the spin-isospin term of the effective interaction is the dominant component. This has also been noted empirically in other charge-exchange reactions, such as the $^{16}\text{O}(p,n)^{16}\text{F}$ study at $E_p=99$ and 135 MeV by Fazely *et al.* [8] and the $^{16}\text{O}(^3\text{He},^3\text{H})$ reaction at 81 MeV by Sterrenburg *et al.* [31]. The fact that the calculated $\Delta J^\pi = 2^-$ cross section is lower by a factor of 2 than the measured differential cross section at $\theta = 0^\circ$ has a drastic consequence in the evaluation of $L = 0$ cross sections, i.e., GT strength, in a multipole decomposition analysis. This has been pointed out by Celler *et al.* [32] in the analysis of the $^{15}\text{N}(n,p)^{15}\text{C}$ reaction at 288 MeV, and by Hicks *et al.* [9] in the analysis of the $^{16}\text{O}(n,p)^{16}\text{N}$ reaction at 298 MeV. In these two cases the authors report difficulty in fitting $L = 1$ angular distributions at forward angles and point out that for this reason a multipole analysis cannot yield a reliable estimate of GT strength in the region of strong dipole transitions. Because of practical considerations, the acceptance of the spectrometer used in the above (n,p) measurements was broad and thus data were reported at averaged scattering angles of 2.0° , 6.4° , and about 11° . The present time-of-flight data in steps of $\Delta\theta = 1^\circ$ between $0^\circ < \theta_L < 4^\circ$ allow a more careful study of this problem. As indicated in the Introduction, one of the advantages of the study of the $^{16}\text{O}(p,n)^{16}\text{F}$ reaction at $E_p=494$ MeV is that it allows data to be obtained at much lower momentum transfer values q , and thus provides more sensitivity to angular distribution shapes near $q = 0$. This is particularly important in the identification of $L = 0$ transitions.

Fazely *et al.* [8] report $^{16}\text{O}(p,n)^{16}\text{F}$ differential cross sections for the excitation of the 2_1^- state in ^{16}F . Data were obtained both at $E_p = 99$ and 135 MeV with neutron energy resolutions of 260 and 310 keV, respectively. We display in Fig. 7 the differential cross sections reported at 135 MeV, plotted versus momentum transfer. The reported values, multiplied by 1.5, are shown together with the present results for the group of low-lying states in ^{16}F . We also present the results [9] obtained in the $^{16}\text{O}(n,p)^{16}\text{N}$ reaction at 298 MeV for the differential cross section exciting the analog states in ^{16}N . All the data points seem to be in a smooth universal curve. The solid line represents the DWIA calculation for the 2^- transition presented in Fig. 6, while the dashed curve represents a similar calculation but with single-particle states bound in a Woods-Saxon potential.

As indicated above, the main contribution to the differential cross section for the first neutron group is due

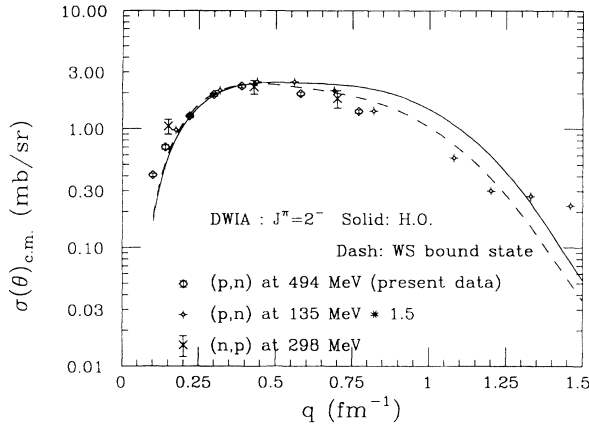


FIG. 7. Differential cross sections for the reactions $^{16}\text{O}(p,n)^{16}\text{F}$ and $^{16}\text{O}(n,p)^{16}\text{N}$ exciting the low-lying group of states near the ground state. The (n,p) data are from Ref. [9] at $E_n=298$ MeV, and the (p,n) data are from our measurements at $E_p=494$ MeV as in Fig. 6. Data at 135 MeV [8] obtained for $^{16}\text{O}(p,n)^{16}\text{F}$ (0.4 MeV 2^-) and multiplied by 1.5 are also included. The solid and dashed curves are DWIA calculations for the 2^- transition assuming HO ($b = 1.726$) and WS bound state wave functions, respectively.

to the 2_1^- transition. Also, the shapes for the 0^- , 1^- , and 2^- calculated transitions are not too different in the $0^\circ < \theta_L < 3^\circ$ interval. Thus we assume that the shape of the measured cross section may be well represented with a calculated 2^- transition. To attempt to understand why the theoretical calculations do not agree with the observed shape of the angular distribution, in this angular interval, DWIA calculations for 2^- transitions were done under different conditions.

The peak of the spin-dipole angular distribution occurs at a momentum transfer $q \sim 0.5$ fm^{-1} ; thus it is expected that near $q \sim 0$ the shape of the calculated angular distribution may be strongly affected by distortions.

We present in Fig. 8 DWIA results for the 2^- transition assuming different optical model parameters.

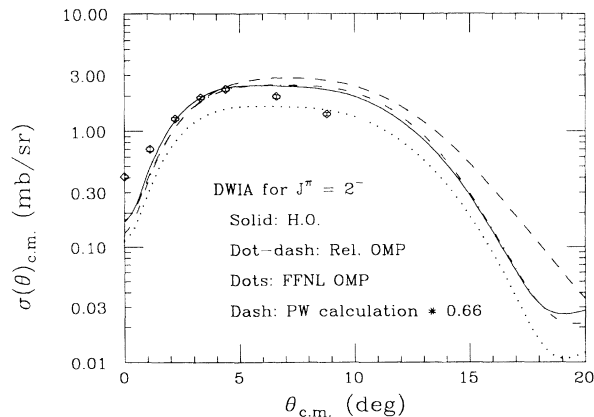


FIG. 8. DWIA calculations for the $^{16}\text{O}(p,n)^{16}\text{F}$ (2_1^-) differential cross section assuming different optical potentials for the incident and outgoing waves. Data are from the neutron group near the ^{16}F g.s., as in Fig. 6.

The solid curve is produced by the same calculation as that for Fig. 7. The dot-dashed curve represents a calculation using a Schrödinger equivalent relativistic potential empirically obtained by fitting proton elastic scattering data in the 21–1040 MeV energy range [25]. The curve represented with dots was obtained using an optical potential obtained in a full-folding nonlocal (FFNL) analysis [33] while the dashed curve is a PWIA calculation multiplied by 0.66 to normalize to the other calculations. It is clear from this exercise that the different optical potentials have almost no effect on the shape of the calculated 2^- angular distribution at $E_p=500$ MeV.

The sensitivity on the different components of the Franey-Love [23] effective interaction is presented in Fig. 9 where central (dashed curve), spin orbit (dot-dashed curve), tensor (squares), and the coherent sum (solid curve) indicate their relative shape and magnitude. From this figure we can infer that the spin-orbit contribution in the effective interaction is negligible while the shape of the 2^- angular distribution for angles less than about 7° ($q \leq 0.6$ fm^{-1}) is dominated by the central interaction. For small angles the data seem to indicate a preference for a stronger tensor interaction than the one used by Franey and Love, while at larger angles ($\theta_{c.m.} > 6^\circ$) a stronger tensor interaction would cause even worse disagreement with the data.

We also studied the sensitivity of the shape of the angular distributions for angles less than $\theta_{c.m.}=5^\circ$ to the shape of the single-particle wave functions. In Fig. 10 calculations assuming HO single-particle states with a range of HO parameter values are presented. A calculation with WS bound state single particles has been presented in Fig. 7. In all cases we note almost no sensitivity in the calculated angular distribution at forward angles to reasonable variations in the bound state wave functions.

Finally, we studied different particle-hole (p-h) configurations for the 2^- transition. The calculations for five

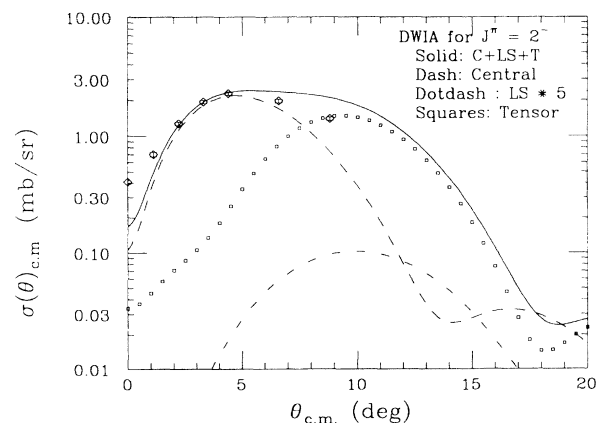


FIG. 9. DWIA calculations for the $^{16}\text{O}(p,n)^{16}\text{F}$ (2_1^-) transition using the Franey-Love effective interaction. The curves represented by dashed and squares represent the central and tensor contributions, respectively. The spin-orbit contribution is much weaker and is represented with the dot-dashed curve after being multiplied by 5. The solid line is the coherent addition of all contributions. Data are the same as in Fig. 6.

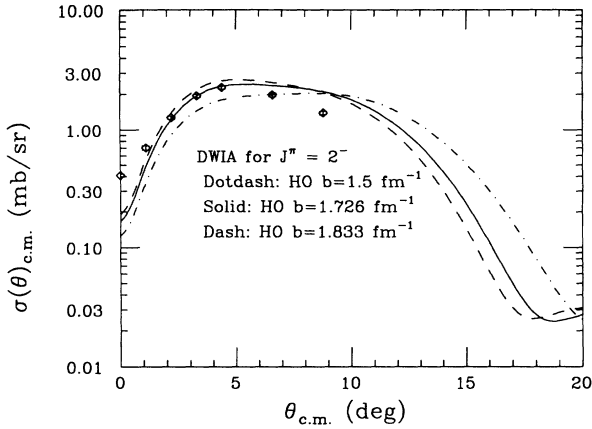


FIG. 10. DWIA calculations for the $^{16}\text{O}(p,n)^{16}\text{F}$ (2_1^-) transition calculated with the indicated values for the HO parameter b . Data are the same as in Fig. 6.

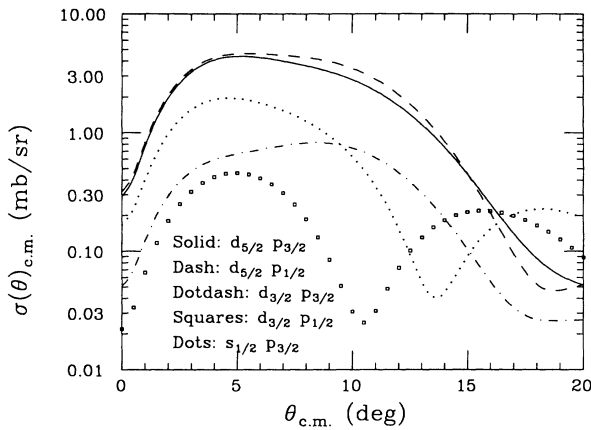


FIG. 11. DWIA calculations for the $^{16}\text{O}(p,n)^{16}\text{F}$ (2_1^-) transition calculated assuming the indicated 1p-1h configuration.

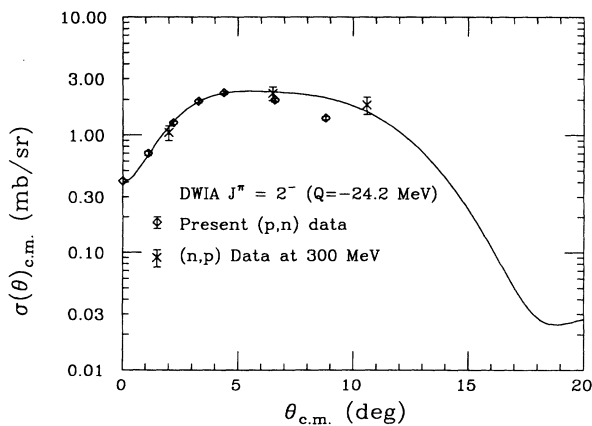


FIG. 12. DWIA calculations for the $^{16}\text{O}(p,n)^{16}\text{F}$ (2_1^-) transition calculated assuming a Q value 8 MeV more negative. Data points obtained in the present study and the $^{16}\text{O}(n,p)^{16}\text{N}$ data points for the analog transitions reported in [9] are shown.

possible configurations are presented in Fig. 11, and all have a similar shape in the forward angles.

In order to perform the multipole decomposition analysis, it was realized empirically that a DWIA calculation assuming a 2^- transition with a Q value 8 MeV more negative than the corresponding Q value for the 0.4 MeV has a shape similar to the data. Such a calculation is presented in Fig. 12 and compared both with the present $^{16}\text{O}(p,n)^{16}\text{F}$ data and the $^{16}\text{O}(n,p)^{16}\text{N}$ data for the analog transitions reported in Ref. [9]. There is no *a priori* reason why this procedure produces the right empirical shape. However, if we assume it needs to be done for “all” the 2^- transitions, a multipole decomposition analysis may produce more reliable results. This is presented in the next section.

2. Multipole decomposition analysis

The shapes of the empirical angular distributions are characterized by ΔJ^π transfers. However, the small differences in shapes among the members of a given calculated ΔL transfer and the limited angular range of the present set of data are not enough to determine individual ΔJ^π ($\Delta J = \Delta L + \Delta S$) contributions. Thus we report the results of the multipole decomposition (MD) analysis by grouping all ΔJ^π transitions to the lowest ΔL value. As such we assume $\Delta L = 0$ for the $\Delta J^\pi = 1^+$ transitions, $\Delta L = 1$ for the $\Delta J^\pi = 0^-, 1^-$, and 2^- transitions. The available data extend only up to $\theta_{c.m.} = 8.8^\circ$, so angular distributions characterized with $\Delta L \geq 2$ are not easily distinguishable. To identify the different ΔL contributions to the measured differential cross section, we have performed a MD analysis [34,35] using a code developed by Park [36]. The center-of-mass double differential cross section data, binned in 0.4 MeV excitation energy steps, were fitted with DWIA calculated differential cross section shapes characterized by a ΔJ^π transfer and also prepared in 0.4 MeV energy intervals, using a least-squares fit technique. Although the data are available in 0.2 MeV energy intervals, the choice of 0.4 MeV intervals (which is about 1/3 of the attained energy resolution) provided a smoother fit and was good enough to distinguish the peaks of interest.

We have calculated angular distributions for ΔJ^π transfers with all possible 1p-1h configurations for the following final J^π states: $1^+(\Delta L = 0)$; $0^-, 1^-$, and $2^-(\Delta L = 1)$; $2^+(\Delta L = 2)$; and $3^-(\Delta L = 3)$. Calculated shapes of the angular distributions are shown in Fig. 13. The shapes in the angular range being considered here are not much affected by the assumption of the 1p-1h configuration involved in a given transition. The DWIA calculations were done in 5 MeV excitation energy intervals between 0 and 30 MeV and an interpolation routine was used to provide the necessary shapes for the energy bins used in the MD analysis. As mentioned in the previous subsection, DWIA calculations for all the 2^- transitions were done assuming an 8 MeV more negative Q value. All other calculations were done with the proper Q value.

For each 0.4 MeV excitation energy interval, the empir-

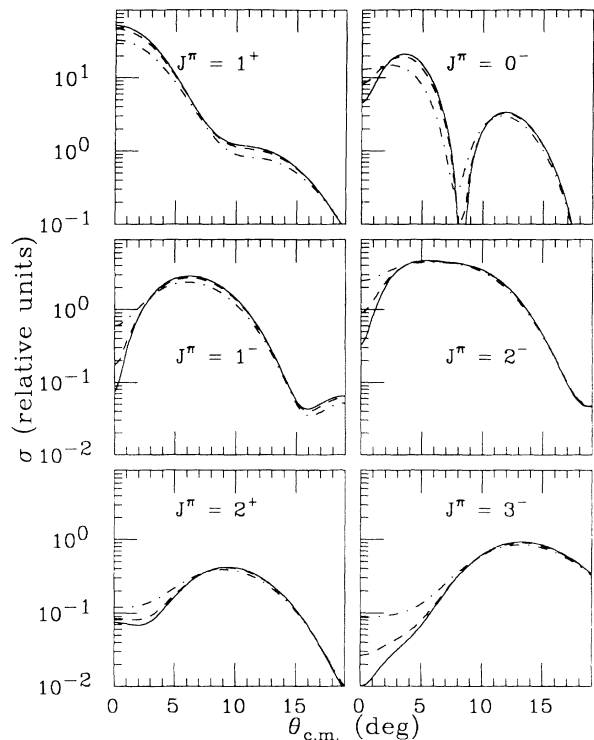


FIG. 13. Calculated relative DW differential cross sections for the indicated ΔJ^π transitions. In all cases calculations are presented for E_x values of 0.0 (solid), 10.0 (dot-dashed), and 30.0 MeV (squares), respectively.

ical angular distributions were least-squares fitted with different combinations of calculated angular distributions weighted with a fitting coefficient, and the set of positive coefficients giving the minimum error was chosen. In Fig. 14 we present some of the results of the decomposition analysis. It is clear that in spite of using a Q -shifted calculation (see Fig. 12) for the 2_1^- transition, the several 0.4 MeV energy bins that constitute the width of that neutron group do not have the same shape as the sum cross section, suggesting the presence of a small admixture of $L = 0$ in the excitation energy region below 2 MeV. Note that a similar problem was present in the MD analysis of the $^{16}\text{O}(n,p)^{16}\text{N}$ data reported in Ref. [9].

3. GT energy distribution

The zero-degree $L = 0$ spectrum obtained in the MD analysis has been corrected to $q = 0$ to obtain the GT energy distribution. The unit cross section value $\hat{\sigma}_{\text{GT}} = 6.6$ mb/(sr GT units), obtained below in Sec. III C, has been used to obtain the distribution presented in Fig. 15. An estimated value $\sum B(\text{GT}) = 1.2$ units is found up to about 30 MeV of excitation in ^{16}F .

It is to be noted that the shape presented in Fig. 15 is very much dependent on the assumed shape for the 2^- transitions. Thus we agree with Celler *et al.* [32] that this method does not provide a completely reliable estimation of the GT strength until we have a better under-

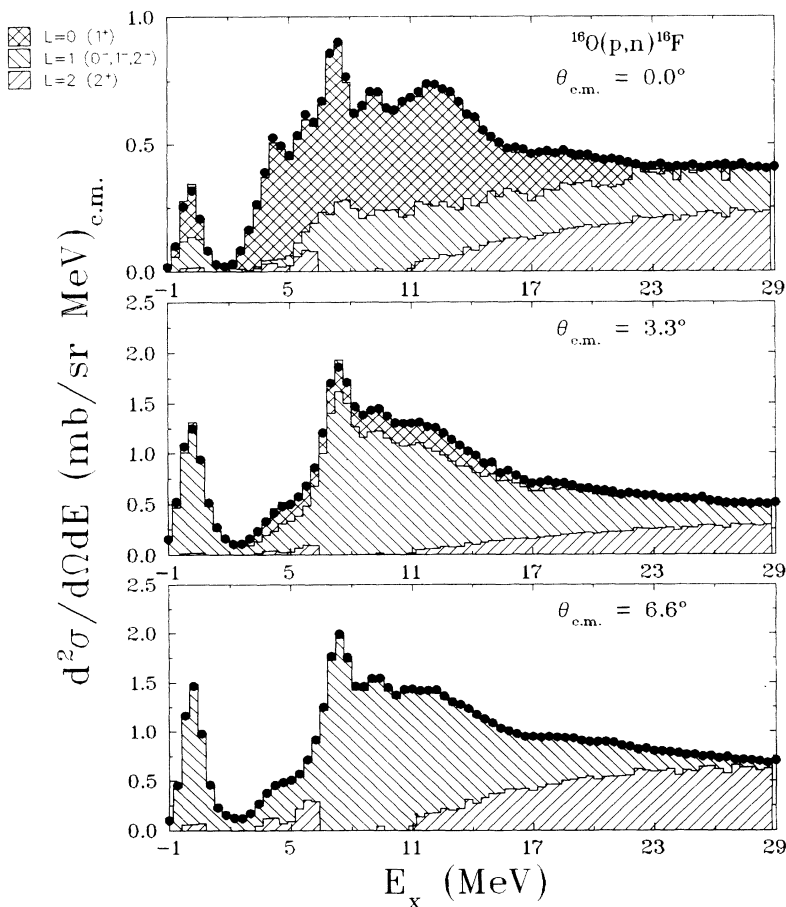


FIG. 14. Results of the multipole decomposition analysis at the indicated angles. Note that the area indicated with $L = 2$ includes contributions with $L \geq 2$.

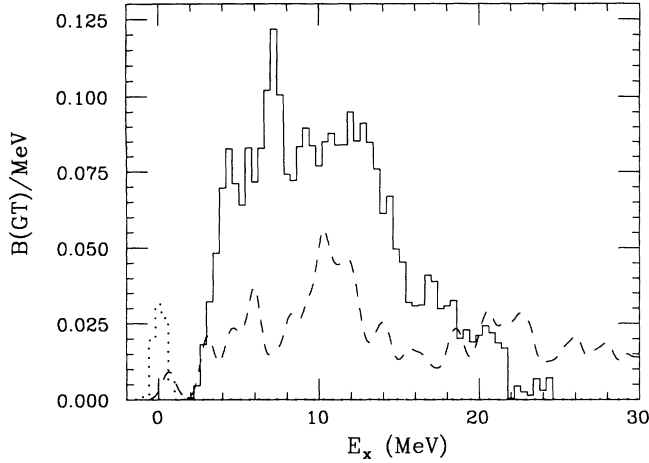


FIG. 15. Gamow-Teller strength distribution (solid histogram) obtained from the 0° $L = 0$ spectrum estimated in the MD analysis. The region near $E_x = 0$ is spurious (see text), and appears dotted. The estimated theoretical GT strength distribution [2] is indicated as a smooth dashed curve.

standing of the discrepancy between experimental and DWIA calculations for spin-dipole transitions. In Fig. 15 we also present as a dashed curve the theoretical GT energy distribution estimated by Haxton and Johnson [2]. The predicted summed GT strength of about 0.7 unit is somewhat smaller than the present estimation of 1.2 unit. However, considering the uncertainties associated with the assumed shapes for the 2^- transitions, the above values for the summed GT strengths and the value reported in the $^{16}\text{O}(n,p)^{16}\text{F}$ study [9] are considered to be in fair agreement.

4. Dipole and spin-dipole energy distribution

We present in Fig. 16 the MD analysis results for transitions characterized with angular momentum transfer $L = 1$ at $\theta_{c.m.} = 4.4^\circ$ as a solid histogram. We also have performed $1\hbar\omega$ DWIA calculations for 0^- , 1^- and 2^- 1p-1h transitions, using the OBDME obtained by Millener [30]. The locations of the contributing states are indicated by dot-dashed ($J^\pi = 0^-$), dashed ($J^\pi = 1^-$), and solid ($J^\pi = 2^-$) vertical lines, respectively. We also have assumed an experimental resolution of 1.2 MeV folded in as a Gaussian distribution, to add the calculated cross sections. This procedure results in the dashed curve of Fig. 16. The general features of the measured spectrum are reproduced by the calculation, in particular the location of the strong 2^- spin-dipole states at excitation energies of 0.4 MeV and 7.5 MeV, respectively. It is clear that at higher excitation energies the calculations do not reproduce the data, probably due to admixtures in the wave function of final states not considered in this simple 1p-1h model. In particular, the calculated strength of the 1^- transition at 12.9 MeV excitation energy is not reproduced by the data. The model also predicts a sizable cross section to a $J^\pi = 0^-$ state at 13.6 MeV with

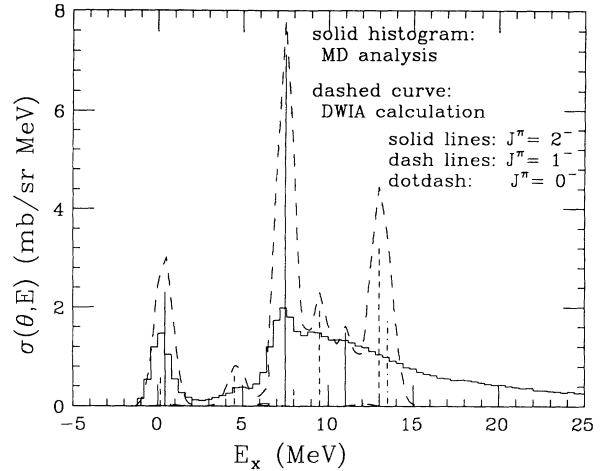


FIG. 16. Calculated spectrum of the $L = 1$ strength from DWIA calculations of $^{16}\text{O}(p,n)^{16}\text{F}$ with Millener-Kurath wave functions for an experimental resolution of 1.2 MeV (dashed curve) compared with multipole decomposition analysis spectrum obtained for $L = 1$ transitions (solid histogram) at $\theta_{c.m.} = 4.4^\circ$. Vertical lines represent locations of calculated states with the indicated J^π value.

mainly a $d_{3/2}p_{3/2}^{-1}$ p-h configuration. With just cross section data, we are unable to distinguish this transition; however, measurements of spin-transfer coefficients such as D_{ij} may be able to distinguish this important true pionic mode of excitation.

C. The $^{18}\text{O}(p,n)^{18}\text{F}$ reaction

To obtain a reliable GT unit cross section $\hat{\sigma}_{GT}$, we also studied the $^{18}\text{O}(p,n)^{18}\text{F}$ reaction measured under identical experimental conditions. The main feature of the 0° spectrum is the strong excitation of the g.s. transition which corresponds to a GT transition with a known beta decay GT matrix element. The ^{18}F positron decay is entirely to the ground state of ^{18}O and has $\log ft = 3.554$ [37]. With a value $g_A/g_V = 1.254$, this implies that $B(\text{GT}) = 3.27$ for the $^{18}\text{O}(p,n)^{18}\text{F}(\text{g.s.})$ transition. In our neutron energy spectrum (Fig. 5) we are unable to separate from this g.s. transition the small contributions due to the 3^+ state at 0.94 MeV, the 0^+ isobaric analog state (IAS) at 1.04 MeV, a rather weak 0^- transition to a 1.08 MeV state, the 5^+ state at 1.12 MeV, and the GT transition to a 1^+ state at 1.70 MeV. The last of these has an estimated $B(\text{GT})=0.195$, as measured by Anderson *et al.* [38] using the $^{18}\text{O}(p,n)^{18}\text{F}$ reaction at 135 MeV.

The angular distribution for the integrated neutron yield up to 2.0 MeV of excitation in ^{18}F is shown in Fig. 17. DWIA curves for the main components to the cross section are also shown on this graph: the GT ground state transition, the IAS Fermi transition, and the GT transition to the 1.7 MeV state. Contributions from higher multipolarity transitions are considerably smaller than those indicated, especially at 0° . The OBDME's were obtained from a calculation with the shell

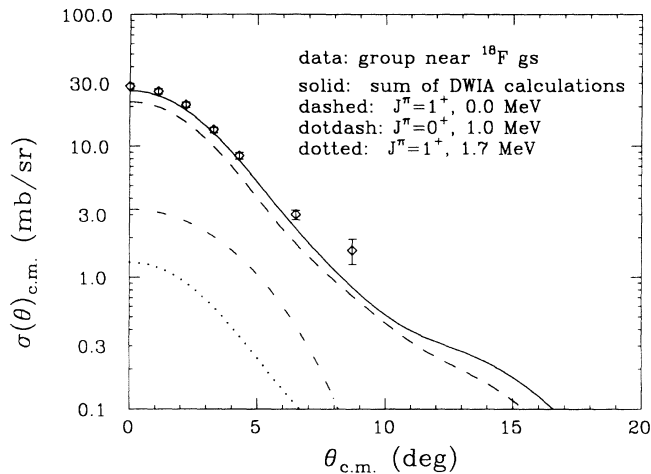


FIG. 17. Angular distribution results for the neutron group near the g.s. of ^{18}F obtained in the $^{18}\text{O}(p, n)^{18}\text{F}$ reaction. This group includes several unresolved states below $E_x = 2.0$ MeV. DWIA calculations for GT transitions (0.0 and 1.7 MeV states) and the IAS Fermi transition (1.04 MeV) are presented. Some weaker transitions are below scale. The solid curve indicates the summed calculation.

model OXBASH. Differential cross sections calculated for GT transitions are normalized so that the $B(\text{GT})$ values used in the DWIA calculation agree with the empirical values of 3.27 and 0.195 mentioned above. The calculation for the Fermi transition is not renormalized.

An overall good agreement with the measured yield is noted. The DWIA calculated value for the unit cross section is $\hat{\sigma}_{\text{GT}} = 6.6$ mb/sr with an estimated 10% uncertainty. Since our data agree very well with the DWIA sum curve at $\theta_{\text{c.m.}} = 0^\circ$, we use $\hat{\sigma}_{\text{GT}} = 6.6$ mb/sr for computing $B(\text{GT})$ strength estimates for both the $^{16}\text{O}(p, n)^{16}\text{F}$ and $^{18}\text{O}(p, n)^{18}\text{F}$ reactions. This unit value is in agreement with the value $\hat{\sigma}_{\text{GT}} = 7.4$ mb/sr reported by Anderson *et al.* [38] at 135 MeV considering the energy dependence of the GT interaction [39]. It should be noted that an erratum to the cross section values reported by Anderson has been published by Watson *et al.* [40] (see Ref. 7 in that publication). Our chosen value is also in agreement with measurements of $\hat{\sigma}_{\text{GT}}$ for the $^{14}\text{C}(p, n)^{14}\text{N}$ reaction near 500 MeV: Sugarbaker *et al.* [39] report $\hat{\sigma}_{\text{GT}} = 5.8 \pm 0.4$ mb/sr, and Alford *et al.* [41] report $\hat{\sigma}_{\text{GT}} = 7.3 \pm 0.5$ mb/sr.

To obtain the $L = 0$ contribution in the 0° spectrum, we have performed a multipole decomposition analysis (see Sec. III B 2). The obtained $L = 0$ results are shown in Fig. 18 where the strength is expressed in units of $B(\text{GT})/\text{MeV}$. We indicate these results only up to 12.5 MeV of excitation energy. A small oil deposit on the front and back windows of the ice target contaminated the spectra with neutrons from the $^{12}\text{C}(p, n)^{12}\text{N}$ reaction, making unreliable the presentation of results beyond that excitation energy. The $L = 0$ results obtained in the MD analysis were extrapolated to $q = 0$ and multiplied by the above unit GT cross section to obtain the GT distribution

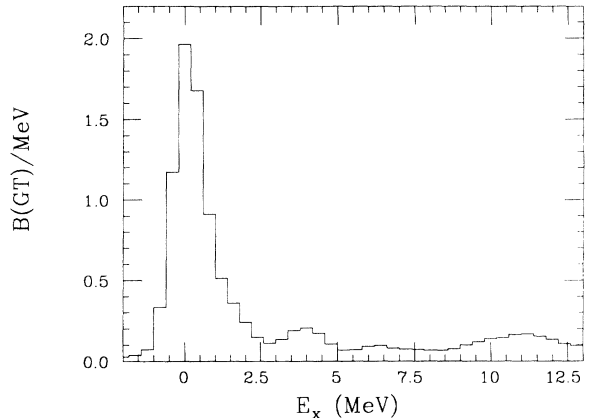


FIG. 18. Gamow-Teller strength distribution obtained from a MD analysis of the $^{18}\text{O}(p, n)^{18}\text{F}$ data.

shown in Fig. 18. A total $\sum B(\text{GT}) = 4.4 \pm 0.5$ sum GT strength is obtained up to 12.5 MeV of excitation, in good agreement with the value $\sum B(\text{GT}) = 3.97 \pm 0.79$ reported by Anderson *et al.* [38].

The code OXBASH [26] was used to obtain transition densities and excitation energies to 1^+ states in ^{18}F . We used a $0\hbar\omega$ calculation within the complete sd -shell-model space and the Brown-Wildenthal interaction [28]. This calculation predicts five states with $J^\pi = 1^+$, $T = 0$ up to 15 MeV of excitation with a total $\sum B(\text{GT}) = 5.445$ unit. About 93% of this strength is contained in the g.s. transition, while 5.2% is predicted for the transition to a state at about 4.0 MeV of excitation. Two other $J^\pi = 1^+$, $T = 1$ states at about 12 MeV of excitation contain an additional $\sum B(\text{GT}) = 0.555$ unit, completing the sum rule (6.0 unit) in this model, which assumes no excitation of the ^{16}O core.

IV. DISCUSSION

The $(0 + 2 + 4)\hbar\omega$ model of ^{16}O [2] predicts the fragmentation of the GT strength in a broad region of excitation energy. We have presented a multipole decomposition analysis of the differential cross section for the $^{16}\text{O}(p, n)^{16}\text{F}$ reaction to estimate the $L = 0$ and $L = 1$ components of the measured cross section. Using this technique we have found a reasonable agreement with the calculations reported by Haxton and Johnson, as well as the empirical evaluation of the GT strength estimated in the $^{16}\text{O}(n, p)^{16}\text{N}$ reaction and reported in Ref. [9]. However, as was the case in the latter reference, large uncertainties are associated with this result, because of sensitivities to the spin-dipole shapes used in the MD analysis.

Although several attempts were made to reproduce the observed shape of the angular distribution corresponding to the excitation of the quartet of low-lying states in ^{16}F , none of them was successful. As pointed out, the shape is predominantly that of a 2^- transition. It is therefore a pionlike excitation and as such dominated by the lon-

gitudinal component of the $(\sigma \cdot \tau)$ interaction. Recent results for the ratio of the longitudinal to transverse nuclear spin response, obtained from (p, n) quasifree studies [16] at momentum transfer $q = 1.75 \text{ fm}^{-1}$, give no evidence for a predicted enhancement of the spin longitudinal response over the spin transverse response. A relativistic random phase approximation calculation done by Horowitz and Piekarewicz [42], in which the relativistic dynamical reduction of the nucleon mass generates a dynamical suppression of the πNN coupling in the medium, reduces the enhancement of the spin longitudinal response and brings the calculation in closer agreement with the data. Another model proposed by Brown and Wambach [43] includes a density-dependent vector meson mass and nucleon effective mass to reduce significantly the isovector part of the tensor interaction. The result is in good agreement with data for the ratio of the spin response. The ideas presented in these two calculations at $q = 1.75 \text{ fm}^{-1}$ may also be needed at lower momentum transfers ($q < 0.5 \text{ fm}^{-1}$) to provide better agreement with data for calculations involving transitions to pionlike states such as the present 2^- case. The data presented here for the (p, n) angular distribution to the quartet of low-lying states in ^{16}F , measured in steps of $\Delta\theta = 1^\circ$, are an excellent scenario to test these ideas.

Future measurements of spin-transfer coefficients for these types of transitions should also provide valuable information about the longitudinal and transverse spin components in the excitation of these states, and will constrain the effective isovector tensor interaction at low momentum transfer. Recent $(p, n) D_{ij}$ measurements on carbon targets near $q = 0 \text{ fm}^{-1}$ suggest that the exchange tensor strength may be enhanced in certain GT reactions [44].

The multipole decomposition analysis for the $^{16}\text{O}(p, n)^{16}\text{F}$ reaction provided information on the dipole ($J^\pi = 1^-$) and spin-dipole ($J^\pi = 0^-, 1^-, 2^-$) energy distributions in ^{16}F which are compared with results from a simple 1p-1h calculation to indicate excitation energy regions of states with $J^\pi = 2^-$ and 1^- .

The analysis of the GT energy distribution obtained in the $^{18}\text{O}(p, n)^{18}\text{F}$ reaction is in good agreement with a previous analysis [38] indicating that up to 12.5 MeV of excitation in ^{18}F about 75% of the total GT strength has been identified.

This work was supported by grants from the United States Department of Energy, and by the National Science Foundation.

-
- [1] G. E. Brown and A. M. Green, Nucl. Phys. **75**, 401 (1966).
- [2] W. C. Haxton and Calvin Johnson, Phys. Rev. Lett. **65**, 1325 (1990).
- [3] E. K. Warburton, and B. A. Brown, Phys. Rev. C **46**, 923 (1992).
- [4] A. Arima and D. Strottman, Phys. Lett. **96B**, 23 (1980).
- [5] K. A. Snover, E. G. Adelberger, P. G. Ikossi, and B. A. Brown, Phys. Rev. C **27**, 1837 (1983).
- [6] C. Djalali, G. M. Crawley, B. A. Brown, V. Rotberg, G. Caskey, A. Galonsky, N. Marty, M. Morlet, and A. Willis, Phys. Rev. C **35**, 1201 (1987).
- [7] G. K uchler, A. Richter, E. Spamer, W. Steffen, and W. Kn upper, Nucl. Phys. **A406**, 473 (1983).
- [8] A. Fazely, B. D. Anderson, M. Ahmad, A. R. Baldwin, A. M. Kalenda, R. J. McCarthy, J. W. Watson, R. Madey, W. Bertozzi, T. N. Buti, J. M. Finn, M. A. Kovash, and B. Pugh, Phys. Rev. C **25**, 1760 (1982).
- [9] K. H. Hicks, A. Celler, O. Hausser, R. Henderson, K. P. Jackson, B. Pointon, J. Rapaport, M. Vetterli, and S. Yen, Phys. Rev. C **43**, 2554 (1991).
- [10] F. Ajzenberg-Selove, Nucl. Phys. **A460**, 1 (1986).
- [11] W. Bohne, H. Fuchs, K. Grabisch, D. Hilscher, U. Jahnke, H. Kluge, and T. G. Masterson, Phys. Lett. **47B**, 342 (1973).
- [12] J. Rapaport, in *Fundamental Symmetries and Nuclear Structure*, edited by J. N. Ginocchio and S. P. Rosen (World Scientific, Singapore, 1989), p. 186.
- [13] W. C. Haxton, Phys. Rev. C **37**, 2660 (1988).
- [14] J. B. McClelland, D. A. Clark, J. L. Davis, R. C. Haight, R. W. Johnson, N. S. P. King, G. L. Morgan, L. J. Rybarczyk, J. Ullmann, P. Lisowski, W. R. Smythe, D. A. Lind, C. D. Zafiratos, and J. Rapaport, Nucl. Instrum. Methods Phys. Res. Sect. A **276**, 35 (1989).
- [15] D. J. Mercer, LANL Report No. LA-12441-MS, 1992.
- [16] X. Y. Chen, T. N. Taddeucci, J. B. McClelland, T. A. Carey, R. C. Byrd, L. J. Rybarczyk, W. C. Sailor, D. J. Mercer, D. L. Prout, S. Delucia, B. Luther, D. G. Marchlenski, E. Sugarbaker, J. Rapaport, E. G lmez, C. A. Whitten, Jr., C. D. Goodman, W. Huang, Y. Wang, and W. P. Alford, Phys. Rev. C **47**, 2159 (1993).
- [17] D. J. Mercer, Ph.D. thesis, University of Colorado, 1992; LANL Report No. LA-12486-T, 1993.
- [18] "Q User's Manual," Los Alamos National Laboratory, Document No. MP-1-3414-2, 1989.
- [19] T. N. Taddeucci, W. P. Alford, M. Barlett, R. C. Byrd, T. A. Carey, D. E. Ciskowski, C. C. Foster, C. Gaarde, C. D. Goodman, C. A. Goulding, E. G lmez, W. Huang, D. J. Horen, J. Larsen, D. Marchlenski, J. B. McClelland, D. Prout, J. Rapaport, L. J. Rybarczyk, W. C. Sailor, E. Sugarbaker, and C. A. Whitten, Jr., Phys. Rev. C **41**, 2548 (1990).
- [20] M. S. Moore, Nucl. Instrum. Methods **169**, 245 (1980).
- [21] C. A. Whitten, Jr., Nucl. Instrum. Methods Phys. Res. Sect. A **309**, 264 (1991).
- [22] R. Schaeffer and J. Raynal, computer code DWBA 70, extended version J. R. Comfort, computer code DW81, Arizona State University, 1984 (unpublished).
- [23] M. A. Franey and W. G. Love, Phys. Rev. C **31**, 488 (1985).
- [24] B. S. Flanders, J. J. Kelley, H. Seifert, D. Lopiano, B. Aas, A. Azizi, G. Igo, G. Weston, C. Whitten, A. Wong, M. V. Hynes, J. McClelland, W. Bertozzi, J. M. Finn, C. E. Hyde-Wright, R. W. Lourie, B. E. Norum, P. Ulmer,

- and B. L. Berman, Phys. Rev. C **43**, 2103 (1991).
- [25] B. Clark and S. Hama (private communication).
- [26] B. A. Brown, A. Etchegoyen, and W. D. M. Rae, The Oxford-Buenos Aires-MSU Shell Model Code (OXBASH), Michigan State University Cyclotron Laboratory, Report No. 524, 1986.
- [27] D. J. Millener and D. Kurath, Nucl. Phys. **A255**, 315 (1975).
- [28] B. A. Brown and B. H. Wildenthal, At. Data Nucl. Data Tables **33**, 347 (1985).
- [29] H. Orihara, S. Nishihara, K. Furukawa, T. Nakagawa, K. Maeda, K. Miura, and H. Ohnuma, Phys. Rev. Lett. **49**, 1318 (1982).
- [30] D. J. Millener (private communication).
- [31] W. A. Sterrenburg, S. Brandenburg, J. H. Van Dijk, A. G. Drentje, M. B. Greenfield, M. N. Harakeh, H. Riezebos, H. Sakai, W. Segeth, S. Y. Van Der Werf, and A. Van Der Woude, Nucl. Phys. **A420**, 257 (1984).
- [32] A. Celler, W. P. Alford, R. Abegg, D. Frekers, O. Häusser, R. Helmer, R. S. Henderson, K. P. Jackson, R. Jeppesen, B. Larson, J. Mildener, B. W. Pointon, A. Trudel, M. Vetterli, and S. Yen, Phys. Rev. C **43**, 639 (1991).
- [33] Ch. Elster, Taksu Cheon, Edward F. Redish, and P. C. Tandy, Phys. Rev. C **41** 814 (1990).
- [34] M. A. Moinester, Can. J. Phys. **65**, 660 (1987).
- [35] K. P. Jackson and A. Celler, in *Spin Observables of Nuclear Probes*, edited by C. J. Horowitz, C. D. Goodman, and G. E. Walker (Plenum, New York, 1988), p. 139.
- [36] B. K. Park, J. Rapaport, J. L. Ullmann, A. G. Ling, D. S. Sorenson, F. P. Brady, J. L. Romero, C. R. Howell, W. Tornow, and C. T. Rönqvist, Phys. Rev. C **45**, 1791 (1992); B. K. Park, Ph.D. dissertation, Ohio University, 1991.
- [37] F. Ajzenberg-Selove, Nucl. Phys. **A475**, 1 (1987).
- [38] B. D. Anderson, A. Fazely, R. J. McCarthy, P. C. Tandy, J. W. Watson, R. Madey, W. Bertozzi, T. N. Buti, J. M. Finn, J. Kelly, M. A. Kovash, B. Pugh, B. H. Wildenthal, and C. C. Foster, Phys. Rev. C **27**, 1387 (1983).
- [39] E. Sugarbaker, D. Marchlenski, T. N. Taddeucci, L. J. Rybarczyk, J. B. McClelland, T. A. Carey, R. C. Byrd, C. D. Goodman, W. Huang, J. Rapaport, D. Mercer, D. Prout, W. P. Alford, E. Gülmez, C. A. Whitten, and D. Ciskowski, Phys. Rev. Lett. **65**, 551 (1990).
- [40] J. W. Watson, W. Pairsuwan, B. D. Anderson, A. R. Baldwin, B. S. Flanders, R. Madey, R. J. McCarthy, B. A. Brown, B. H. Wildenthal, and C. C. Foster, Phys. Rev. Lett. **55**, 1369 (1985) (see Ref. [7] in this publication).
- [41] W. P. Alford, R. L. Helmer, R. Abegg, A. Celler, O. Häusser, K. Hicks, K. P. Jackson, C. A. Miller, S. Yen, R. E. Azuma, D. Frekers, R. S. Henderson, H. Baer, and C. D. Zafiratos, Phys. Lett. B **179**, 20 (1986).
- [42] C. J. Horowitz and J. Piekarewicz, Phys. Lett. B **301**, 321 (1993).
- [43] G. E. Brown and J. Wambach, Report No. KFA-IKP(TH)-1993-04 (unpublished).
- [44] D. J. Mercer, T. N. Taddeucci, L. J. Rybarczyk, X. Y. Chen, D. L. Prout, R. C. Byrd, J. B. McClelland, W. C. Sailor, S. DeLucia, B. Luther, D. G. Marchlenski, E. Sugarbaker, E. Gülmez, C. A. Whitten, Jr., C. D. Goodman, and J. Rapaport, Phys. Rev. Lett. **71**, 684 (1993).